# Rate- and Time-Dependent Mechanical Behavior of Foam-Grouted Coarse-Grained Soils

Johannes Jessen[1] and Roberto Cudmani[2]

**Abstract:** This paper experimentally investigates the mechanical properties of foam-injected gravel by means of uniaxial compression tests and uniaxial creep tests. Bonding of noncohesive soils by foam injection is a novel soil improvement method that can be applied for the stabilization of cohesionless soils at the tunnel face and behind soldier pile walls. Limited data on the mechanical behavior of foam-injected soils is available in the literature. A method for the preparation of homogeneous and reproducible test specimens was developed. The testing program included the variation of the factors that influence the mechanical behavior (e.g., initial soil density, grain size, strain rate, curing time, and stress level). Similar to cemented soils, the foam-injected soils show an elastoplastic stress–strain response and softening beyond the peak. The mechanical behavior is time-, stress- and rate dependent. The strength and stiffness can be described by the porosity–binder concept considering the influence of strain rate, soil density, and foam content. **DOI: 10.1061/(ASCE)GT.1943-5606.0002763.** 

**Author keywords:** Foam; Composite; Bonding; Creep; Porosity–binder concept.



## Introduction

Bonding of granular soil by grouting is a common procedure that is used for ground improvement (Hornich and Stadler 2011; Karol 2003; Cambefort 1969; Kutzner 1991). Soil properties are modified by the addition of a binder agent, which is injected as a fluid into the pores of the granular skeleton (Nicholson 2014). Typical fields of application for bonding of granular soil include underpinnings, foundations, soldier pile walls, and face stabilization in shotcrete tunneling (Bruce et al. 2017; Fillibeck et al. 2006; Garshol 2002; Holter and Hognestad 2012).

Hydraulic binders (e.g., cement and lime) are the most common mixing agents used for soil grouting in geotechnical engineering. In special cases, however, their effectiveness can be severely affected by adverse grout features (e.g., segregation, dilution, and slow setting) as described by Cambefort (1969) and Warner (2004). Particularly, in highly permeable, coarse-grained soils, the use of cementitious grout can be inefficient. Due to the slow setting time, a relatively long flow path is required for the grout to stagnate at a given pumping rate or grout pressure. Consequently, grout losses result in unnecessary high grout consumption. Additionally, there is a significant risk of dilution of hydraulic binders under flowing groundwater (Warner 2004).

To overcome these limitations, grouting technology has recently undergone a rapid development. A variety of polymers have been proposed, particularly foams (Karol 2003). Compared to cementitious grouts, foam injection offers several advantages:

- A significantly shorter setting time (only few minutes after grouting) prevents uncontrolled grout flow out of the target area and significantly reduces dilution under flowing ground water.
- Higher early age strength (more than 80% of the 28-days strength can be reached after a few minutes) enables continuous construction progress (e.g., for the fast stabilization and excavation of the space in between the piles of a soldier pile wall).
- The initial components of foaming grout require little space for storage, which is favorable in limited confines (e.g., tunneling, mines, or structural grouting) (Warner 2004).

Many studies have already been performed in the field of foam injection for soil conditioning in earth pressure balance shield (EPBS) tunneling. In this case, the aim of the foam is to reduce the friction and adhesion of the soil to facilitate soil excavation and soil flow in pipes (Quebaud et al. 1998; Thewes and Budach 2010; Wu et al. 2018; Mori et al. 2018; Liu et al. 2019; Budach and Thewes 2015). However, the function of foam grouting is the opposite (i.e., to enhance the mechanical properties—strength and stiffness—of the soil). As in other composite materials, this is achieved by two main mechanisms: the creation of bonding (cohesion) among the grains and the prevention of dilatancy of the granular skeleton.

Apart from soil conditioning, the application of foam grouting to improve the mechanical behavior of soils, especially coarse-grained soils, has seldom been the focus of geotechnical or material researchers. Only a handful of studies on this topic can be found in the literature.

Bodi et al. (2012) provide a general overview about foaming injection materials, the injection technology, and their applications. Parameters affecting the behavior of soil–foam mixtures are mentioned, but a quantification of the mechanical properties is missing. Scucka et al. (2015) microscopically investigated the structure of polyurethane foam-grouted samples of basalt, brick, and coal slag. They predominantly focused on the parameters of the foam structure and texture, and concluded that the mechanical behavior of the investigated compounds depends primarily on the amount of foam in the pores and the so-called "foam factor" (see following section

[1]Ph.D. Candidate, Dept. of Civil, Geo and Environmental Engineering, Institute of Soil Mechanics and Foundation Engineering, Technical Univ. of Munich, Rock Mechanics and Tunnelling, Franz-Langinger-Str. 10, München 81245, Germany (corresponding author). ORCID: https://orcid.org/0000-0003-2666-7922. Email: johannes.jessen@tum.de

[2]Professor, Dept. of Civil, Geo and Environmental Engineering, Institute of Soil Mechanics and Foundation Engineering, Technical Univ. of Munich, Rock Mechanics and Tunnelling, Franz-Langinger-Str. 10, München 81245, Germany. Email: roberto.cudmani@tum.de

Note. This manuscript was submitted on March 10, 2021; approved on December 15, 2021; published online on February 28, 2022. Discussion period open until July 28, 2022; separate discussions must be submitted for individual papers. This paper is part of the ***Journal of Geotechnical and Geoenvironmental Engineering***, © ASCE, ISSN 1090-0241.

"Foam"). Relatively high compressive strengths ranging from 30 to 90 MPa were determined, but a systematic experimental evaluation of the rate- and time-dependent behavior of the compounds was not carried out.

Apart from these investigations, we are not aware of any experimental research into foam-injected soils, particularly regarding the time- and rate-dependent material behavior of foam-injected coarse-grained soils. To fill this gap, the main purpose of this paper is to investigate the physical properties as well as the time- and rate-dependent mechanical behavior of foam-grouted soil, focusing on the enhancement of the mechanical properties of cohesionless soil. After a description of the materials used in the study, a method for the preparation of homogeneous and reproducible test specimens will be presented. The mechanical behavior of foam-injected coarse-grained soils was investigated by uniaxial compression tests and uniaxial creep tests considering the influence of grain size, initial relative density, curing time, loading history, and strain rate. Finally, the strength and stiffness of the composite are described by the porosity–binder concept considering the influence of strain rate, soil density, and foam content.

## Materials

### Foam

In order to understand the mechanical behavior of the soil–foam composites, it is important to become familiar with the material behavior of the pure foam. Therefore, some of the main features of the mechanical behavior of foams are summarized in this section. In general, solid foams are either composed of open or closed cells. In open-cell foam, the solid material is drawn into separated struts that form the cell edges leading to interconnected gas pockets. In closed-cell foam, the released gas forms discrete pockets, each completely surrounded by solid membranes that close off the cell faces (Gibson and Ashby 2014). As in other porous solids, the mechanical behavior of foams is particularly influenced by the foam density or foam factor (Ashby 1983, 2006; Valentino et al. 2014; Wei et al. 2017; Obi 2018; Maji et al. 1995). The foam density $\rho_{foam}$ is

$$\rho_{foam} = \frac{m_{foam}}{V_{foam}} \tag{1}$$

where $m_{foam}$ is the mass of the foam; and $V_{foam}$ is the volume in the foamed state including the gas-filled cells. The foam factor $f_{foam}$ is the density ratio of the initial fluid components ($\rho_{fluid}$) and the foamed material after expansion ($\rho_{foam}$)

$$f_{foam} = \frac{\rho_{fluid}}{\rho_{foam}} \tag{2}$$

The mechanical behavior of foams is temperature- and rate-dependent (Obi 2018; Tu et al. 2001; Mane et al. 2017; Gibson and Ashby 2014; Richeton et al. 2006). Both dependences result from thermally activated processes at the molecular level, which can be described by the following relationship derived from the rate process theory (Eyring 1936):

$$\dot{\varepsilon} = \dot{\varepsilon}_0 \left(\frac{\sigma}{\sigma_0}\right)^N \quad \text{with} \quad \dot{\varepsilon}_0 = Kexp(-Q/RT) \tag{3}$$

where $\sigma_0$ and $\dot{\varepsilon}_0$ are constants characterising the creep behavior of the solid part of the foam, $K$ is the preexponential factor, $N$ is the creep exponent, $Q$ is the creep activation energy in J/mol, $R$ is the gas constant in 8.313 J/(K/mol), and $T$ is the temperature in K (Andrews et al. 1999a; Diologent et al. 2009; Burteau et al. 2014).

The macroscopic stress–strain behavior of foams during compression is categorized into elastic deflection, buckling, and plastic collapse of the cell walls (Gibson and Ashby 2014; Obi 2018), as presented in Fig. 1(a).

The creep behavior can be divided into three phases—primary, secondary, and tertiary—on the strain–time diagram, as shown in Fig. 1(b). Initially, the strain rate decreases, followed by an almost constant state (steady state). Finally, the strain rate increases with time until a possible densification leads again to a further reduction of the strain rate. For some foams, the secondary creep phase is negligibly short and tertiary creep starts almost immediately after achieving the minimum strain rate (Huang and Gibson 1991). The time to achieve the turning point of the strain rate depends on the initial density and the state of stress (Couteau and Dunand 2008).

In this study, a commercial solid hydrophobic two-component silicate foam was used. The product was provided by TPH Bausysteme GmbH, a German manufacturer of injection materials. The foam was selected for its high foaming factor and fast reaction time. Before grouting, the starting components of the foam were mixed by a volume ratio of 1:1 according to the manufacturer's

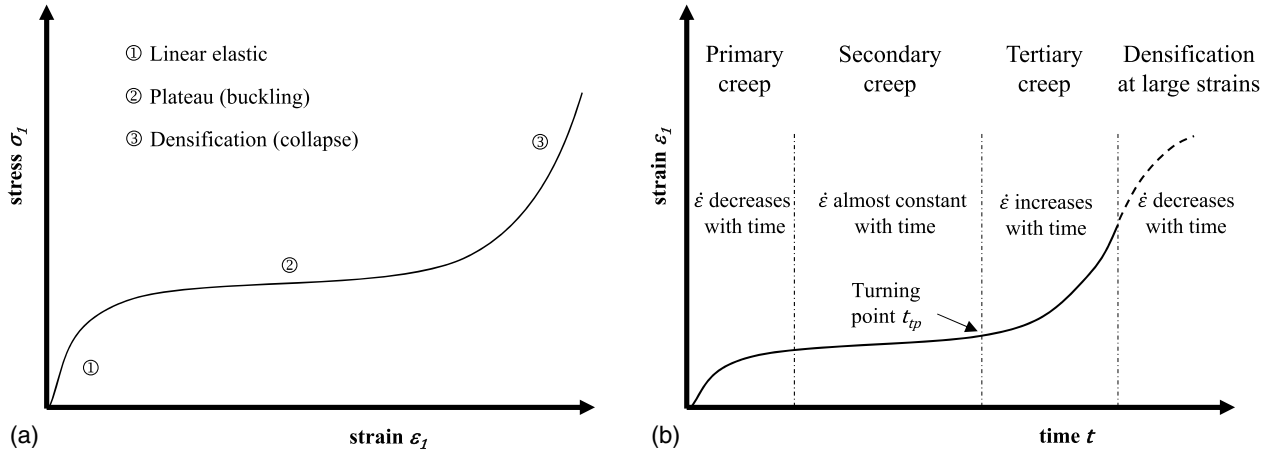


**Fig. 1.** Schematic behavior of foams during compression: (a) stress–strain behavior; and (b) creep curve. [Reprinted from *Acta Materialia*, Vol. 27 (4), E. W. Andrews, J.-S. Huang, and L. J. Gibson, "Creep behavior of a closed-cell aluminum foam," pp. 2927–2935, © 1999, with permission from Elsevier.]

**Table 1.** Properties of the two starting components of the silicate foam

| Component | Chemical base | Density $\rho$ (g/cm$^3$) | Viscosity $\eta$ at 23°C (mPa/s) |
|---|---|---|---|
| A | Sodium silicate glass | 1.30 | 30 |
| B | Polyisocyanat | 1.21 | 120 |

specifications. The flow characteristics and the chemical base of the two components are listed in Table 1.

This mixture cures by chemical reaction ("reaction foams") in the pores of the soil within a few minutes under exothermic conditions. At a temperature of 23°C, the initiation time (cream time)—the time between the start of mixing and the point when fine bubbles begin to appear—is about 45 s, while the end of rise time—the time at which the foam stops expanding—occurs after 90 s. The reaction time and viscosity are strongly temperature dependent; with increasing temperature, the reaction time and viscosity decrease. The foam used in our study can increase its volume by 30 times under free expansion conditions.

Fig. 2(a) shows a microscopic image of the randomly arranged foam structure after free expansion. Three cells are outlined with white dotted lines to highlight the foam structure. Number [1] in Fig. 2(a) indicates a representative cell wall between two cells with thickness of approximately 53 $\mu$m. Fig. 2(b) presents a uniaxial compression test of the silicate foam with elastoplastic material behavior. The uniaxial compressive strength $q_u$, defined as the axial stress $\sigma_1$ for the axial strain of $\varepsilon_1 = 0.1$, is about 0.73 MPa for a foam density of 0.22 g/cm$^3$, which corresponds to a foam factor of 5.5. The axial stiffness $E$ is about 15 MPa in the quasi-linear range of the stress–strain curve.

### Soils

Two natural washed gravels—a fine gravel ($fGr$) and a medium gravel ($mGr$)—were used for the investigations. The soils represent the ground conditions encountered in Munich and the surrounding area, where limitations of cement grouting (e.g., for the stabilization of tunnel faces) have been observed. Figs. 3(a and b) show micrographs of the soils $fGr$ and $mGr$, respectively. Comparing the same scale images in Figs. 3(a and b), the differences in the grain size can be visualized. Both soils come from the same quarry and have similar mineralogy. The grain shape is rounded to angular and the surface texture is rather smooth.

Table 2 summarizes the granulometric properties ($C_U$ uniformity coefficient; $C_C$ curvature number; $\rho_S$ density of solid particles; $e_{max}$ maximum void ratio; $e_{min}$ minimum void ratio; $x_{area}$ mean equivalent diameter; and $S_m$ mass specific surface) and the permeability ($k$ = hydraulic permeability) of the soils.

Besides the difference in grain size, the two soils vary, in particular with regard to their mass-specific surface area $S_m$ and their hydraulic permeability $k$. The mass-specific surface area of the soil $fGr$ is about 2.3 times higher than that of the soil $mGr$. Assuming an ideal spherical particle shape, the mass specific surface was approximated according to Stieß (2009) by

$$S_m = \frac{6}{\rho_s \cdot x_{area}} \tag{4}$$

where $x_{area}$ is the diameter of a circle having the same projection area $A$ as the grain, demonstrated in Fig. 4(a). The grain size distributions of the soils in Fig. 4(b) and the mean equivalent diameter of the particles $x_{area}$ were investigated by means of a Camsizer Analysis (Microtrac Retsch GmbH 2021).

For subsequent comparison with the foam-grouted soil, triaxial tests were examined on the natural soil (without foam). Fig. 5 shows the results of consolidated, drained triaxial tests on the two gravels for a confining pressure of $\sigma_3 = 100$ kN/m$^2$. The samples of the soils $fGr$ and $mGr$ were prepared in a medium-dense state with a relative density $I_D$ of 0.55, according to Eq. (5)

$$I_D = \frac{e_{max} - e}{e_{max} - e_{min}} \tag{5}$$

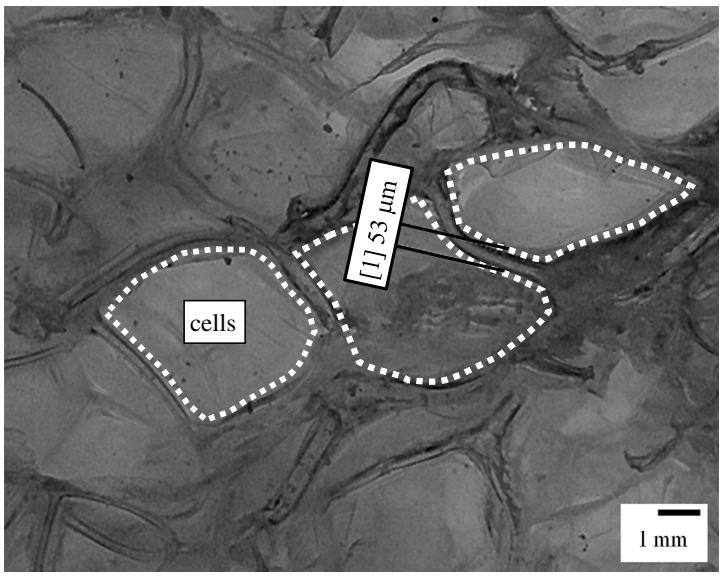


(a)

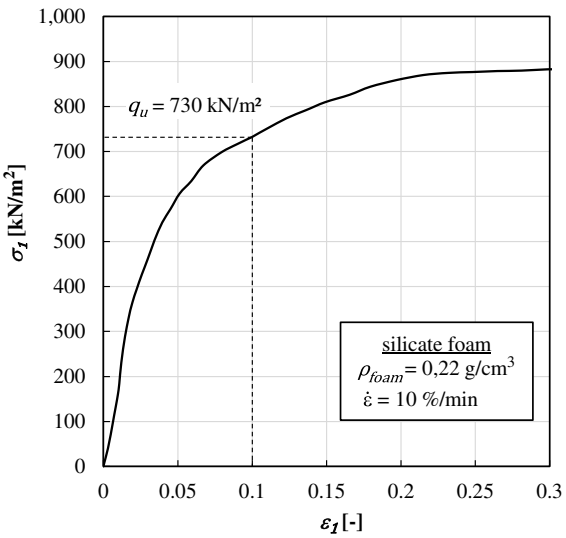


(b)

**Fig. 2.** (a) Microscopic image of the silicate foam after free expansion; and (b) uniaxial compression test of the silicate foam for $\rho_{foam} = 0.22$ g/cm$^3$ (TPH Bausysteme GmbH, unpublished data, 2018).

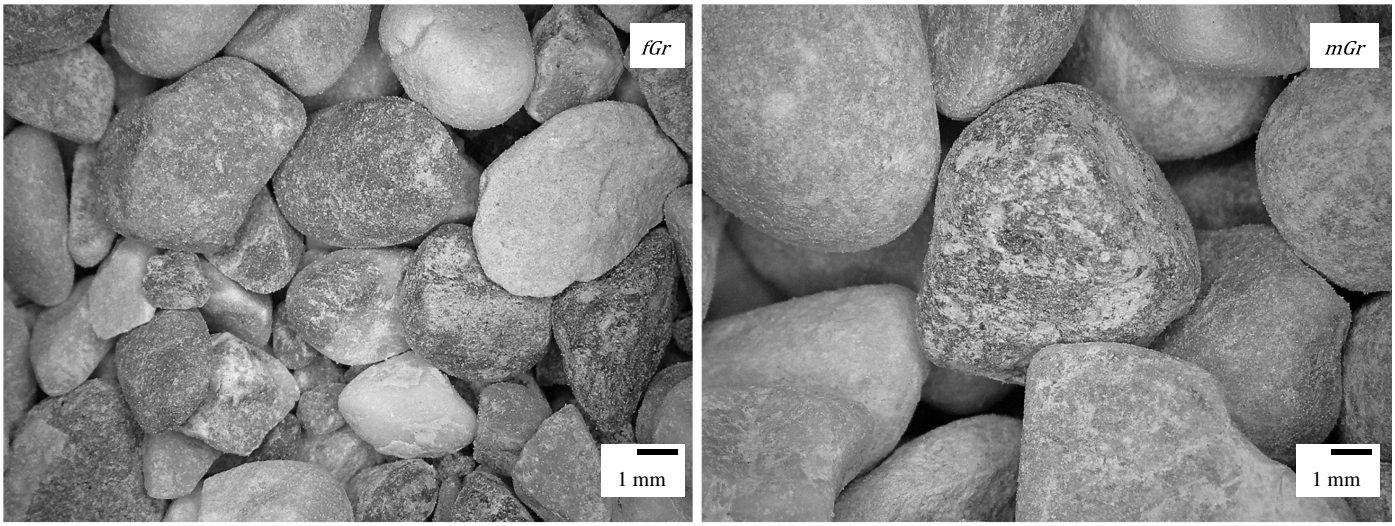


**Fig. 3.** Optical micrographs of the natural soils: (a) $fGr$; and (b) $mGr$.

**Table 2.** Classification characteristics of investigated materials

| Soil | $C_U$ | $C_C$ | $\rho_S$ (g/cm$^3$) | $e_{max}$ | $e_{min}$ | $x_{area}$ (mm) | $S_m$ (cm$^2$/g) | $k$ ($e_{max}$) (m/s) | $k$ ($e_{min}$) (m/s) |
|---|---|---|---|---|---|---|---|---|---|
| $fGr$ | 2.0 | 1.0 | 2.760 | 0.716 | 0.470 | 3.48 | 6,247 | $1.8 \times 10^{-2}$ | $6.0 \times 10^{-3}$ |
| $mGr$ | 1.4 | 1.0 | 2.744 | 0.691 | 0.499 | 8.09 | 2,703 | $2.3 \times 10^{-1}$ | $9.1 \times 10^{-2}$ |

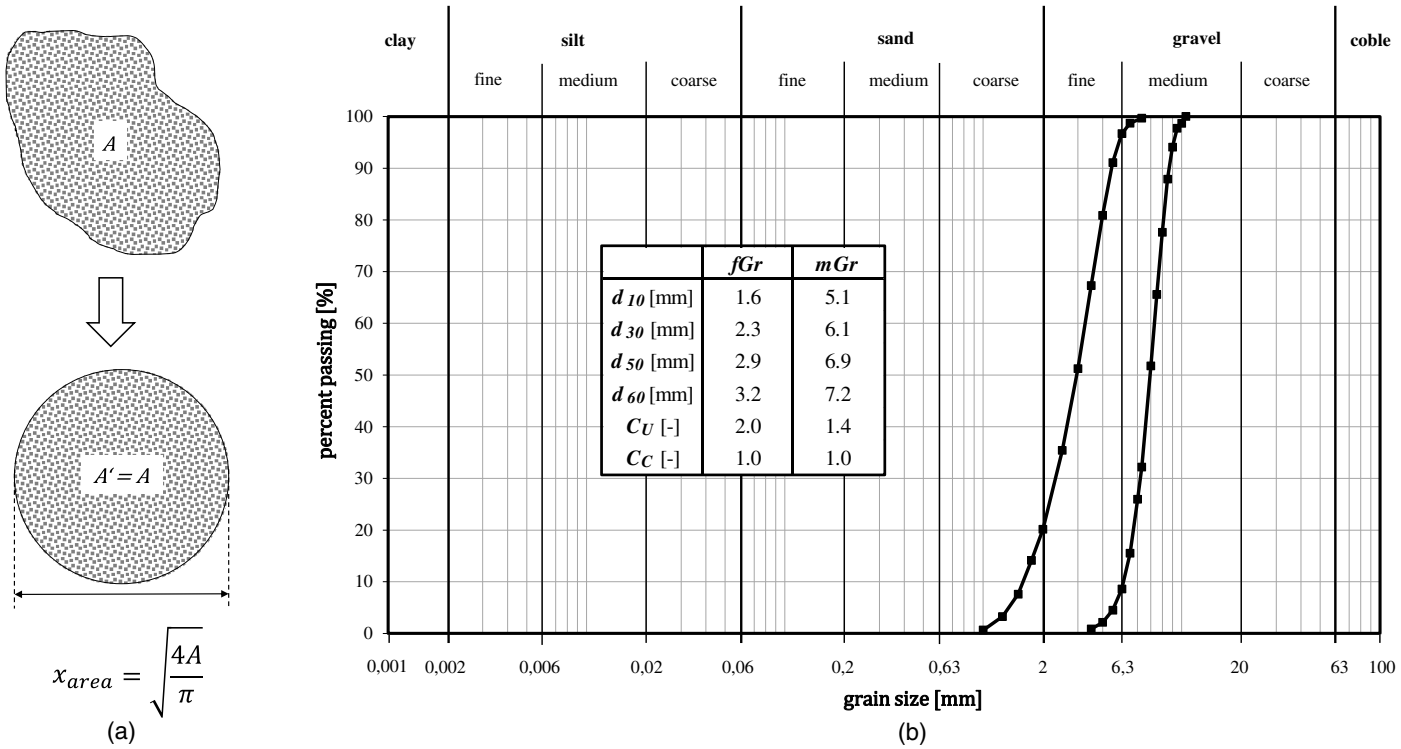


**Fig. 4.** (a) Definition of $x_{area}$ of Camsizer-analysis (reprinted with permission from Microtrac Retsch GmbH 2021); and (b) GSDs of investigated soils: $fGr$ and $mGr$.

Then, the samples were saturated and consolidated before shearing with a constant rate of strain ($\dot{\varepsilon} = 0.05\%/\text{min}$). The diameter of the samples was $D = 100$ mm. The observed stress–strain and volumetric behavior of the natural soils are similar. As expected, strength (peak of deviator stress), prepeak stiffness, and dilatancy were slightly higher for the coarser soil $mGr$. The results in Fig. 5 can be used as a reference for assessing the enhancement of material properties by foam injection.

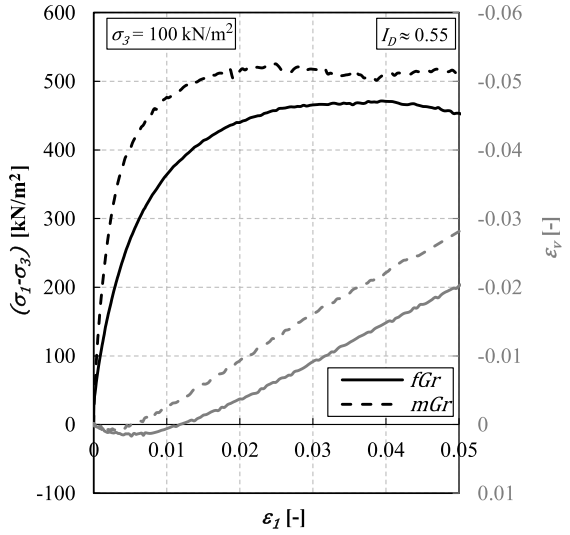


**Fig. 5.** Consolidated drained triaxial tests on the soils *fGr* and *mGr*.

## Experimental Program on Foam-Injected Soil and Experimental Setup

The experimental program on foam-grouted composites involved uniaxial compression tests with a constant rate of strain and uniaxial creep tests at different stress levels. The laboratory tests were performed based on European standard ISO 17892-7 (DIN 2018). Geotechnical investigation and testing– Laboratory testing of soil—Part 7: Unconfined compression test. In some of the uniaxial compression tests, unloading/reloading loops were carried out to evaluate their influence on the behavior. Based on the laboratory test results, the following factors influencing the mechanical behavior of foam-grouted specimens were investigated: relative density $I_D$, curing time $t_{cu}$, strain rate $\dot{\varepsilon}$, and grain size.

The tests were carried out in a computer-controlled electromechanical load-frame driven by a stepper-motor using a 100 kN s-shape load cell and an incremental deformation transducer with a resolution of 0.00025 mm. During the uniaxial compression tests with different grain size, the volumetric deformation behavior of the test specimens was examined with the help of circumferential deformation sensors. The circumferential extensometers were installed in the quarter points of the test specimens, as shown in Fig. 6.

The circumferential deformation measuring device used consists of a prestressed roller-chain that can be elongated by means

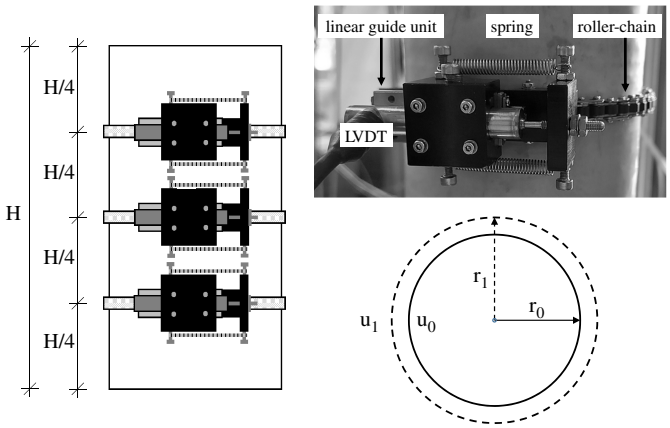


**Fig. 6.** Circumferential measurement device.

of a linear guide unit. An inductive sensor (LVDT) is attached to the roller chain by means of a casing. The LVDT features a measuring range of 10 mm and provides an accuracy of 0.05 mm. The casing guarantees frictionless movement of the core extension rod inside the LVDT core. The radial and volumetric deformations can be determined from the change of the circumference by

$$\Delta u = 2\pi(r_1 - r_0)(r_1 - r_0) = \Delta u/(2\pi) \tag{6}$$

$$(r_1 - r_0)/r_0 = \Delta u/(2\pi r_0)\varepsilon_3 = \Delta u/(2\pi r_0) \tag{7}$$

$$\varepsilon_v = \varepsilon_1 + \varepsilon_3 + \varepsilon_3 = \varepsilon_a + 2\varepsilon_3 \tag{8}$$

Cylindrical test specimens with restrained ends typically do not deform homogenously. The samples bulge in the middle and assume the shape of a barrel. Vertical, lateral, and volumetric strain distributions as well as the stress distribution inside the specimen become nonuniform. Therefore, the analysis of test results is complicated (Lade 2016). For evaluation of the radial deformations, the central LVDT was used because the influence of end restraint is minimal in the middle of the test specimen. Typical geotechnical sign convention—contraction positive—is chosen. For the determination of the axial stress, the current cross-sectional area was calculated according to Lade (2016) by

$$A = A_0(1 - \varepsilon_3)^2 \tag{9}$$

### Specimen Preparation

A test rig for the production of test specimens was designed and optimized on the basis of several preliminary investigations and literature references (Christopher et al. 1989; Gartung 1976). The experimental test setup consists of a 50-cm-long plastic pipe made of PVC (DN 110), which is screwed to a wooden frame for fixing with pipe clamps [Figs. 7(a–c)].

The air-dried soil was filled in the tube in layers by dry funnel deposition. The target value of the relative density $I_D$ was achieved by mechanical compaction in the way of systematic blows with a wooden mallet. To avoid swelling of the granular skeleton during foam expansion, a perforated steel plate was placed on the top of the sample and its motion was restrained by two bolts fixed at the top of the pipe. The bottom and top plates were perforated with drainage holes, enabling the escape of the displaced air. Using a compressed air-driven cartridge gun, 300 mL each of the liquid A- and B-component were combined in a static mixer and injected at a pressure of 2.85 bar. One hour after injection, the tubes were cut longitudinally on two opposite sides to remove the samples. Afterward, the test specimens were cut to size with a dry cutting stone saw. The injection, curing, and testing of specimens were performed under constant temperature conditions. Fig. 8 shows an example of a final test specimen with the cut end face. The sample size in the uniaxial compression and the uniaxial creep tests was 110 mm in diameter and 220 mm in height ($H/D \approx 2.0$).

### Repeatability and Validation of Specimen Preparation

Before starting the testing series, various tests were carried to demonstrate sample preparation repeatability. Fig. 9 shows two uniaxial compression tests on foam grouted *fGr* under the same test conditions ($I_D = 0.5$; $\dot{\varepsilon} = 1.0\%/\text{min}$; $t_{cu} = 2$ h). The stress–strain relationship up to the peak is almost identical in both tests. Even during unloading and reloading, no significant difference was discernible between the two tests. Only after exceeding the uniaxial strength, the test curves slightly deviate due to the formation of cracks and shear localization. Nonetheless, both curves qualitatively show the

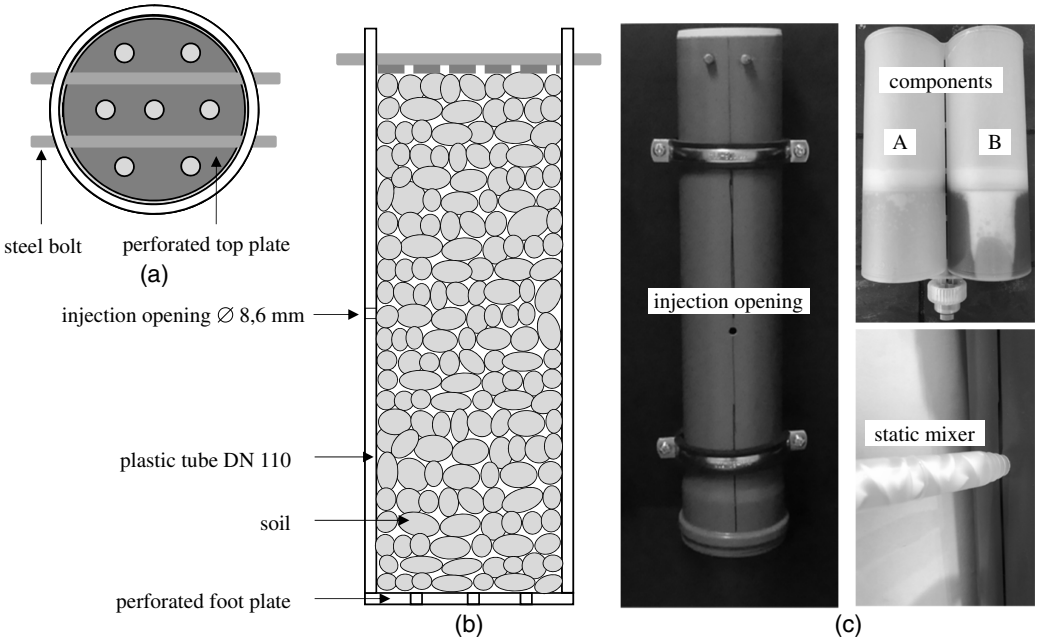


**Fig. 7.** Experimental setup for specimen preparation: (a) top view; (b) cross-sectional view; and (c) photographs.

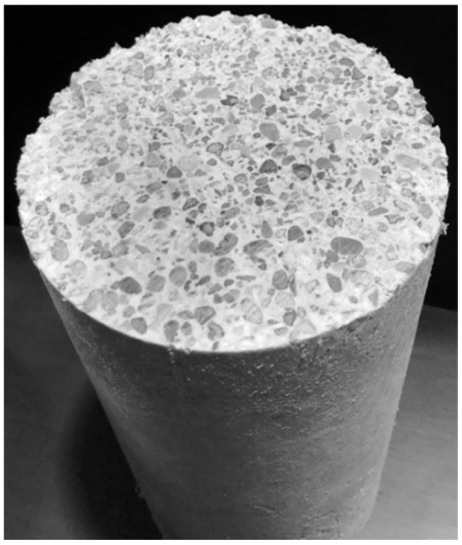

**Fig. 8.** Test specimen of foam-injected $fGr$ with cut end face $H/D = 2$.

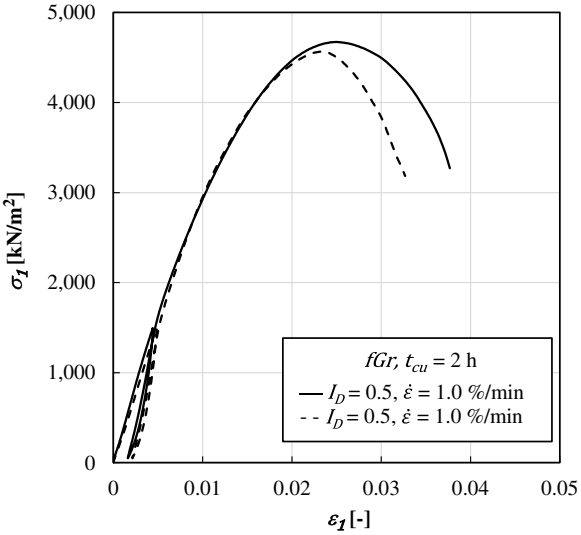


**Fig. 9.** Two identical uniaxial compression tests on samples of foam-grouted $fGr$ to show repeatability of the sample preparation and the experimental results.

same behavior beyond the peak. Because for practical application of foam-grouting, the stress–strain behavior up to the peak is decisive, the result confirms the adequacy of the developed sample preparation technique.

### *Stress–Strain Behavior*

According to Fig. 9, the typical stress–strain behavior of the foam-injected specimens under uniaxial compressive stress can be characterized as follows.

At the beginning of loading, the curves show a slightly concave increase, which is caused by the unevenness and imperfect parallelism of the specimen end faces. Afterward, the stress–strain relationship is approximately linear. However, with increasing strain, the behavior becomes increasingly nonlinear, indicating crack initiation. As the axial load continues to increase, the cracks expand and grow until a fracture structure finally forms and the maximum stress is reached. The permanent deformation during unloading indicates irreversible structural damage. Plastic strains occur even at lower stresses.

## Uniaxial Compression Tests

### *Influence of the Initial Relative Density*

At first, a test series of uniaxial compression tests on foam-grouted $fGr$ with different initial relative densities ($I_D = 0.15$ loose, 0.5

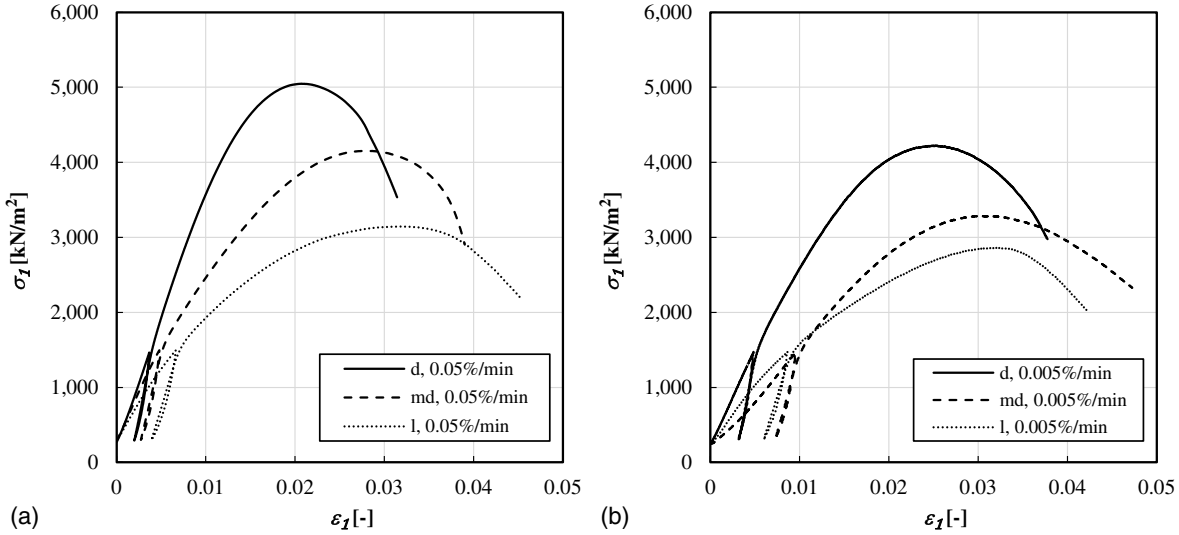


**Fig. 10.** Uniaxial compression tests of foam-injected $fGr$ with varying initial densities at constant strain rates: (a) 0.05%/min; and (b) 0.005%/min.

medium dense, 0.85 dense) was performed at loading strain rates of $\dot{\varepsilon} = 0.05\%/\text{min}$ and $\dot{\varepsilon} = 0.005\%/\text{min}$. The stress–strain curves are presented in Figs. 10(a and b).

The test results show that the influence of the relative density $I_D$ on the uniaxial compressive resistance is significant for both considered strain rates. The lower the relative density, the lower the compressive strength and the more ductile the samples behave. Due to the larger pore volume of the loose samples in comparison with the dense samples, the foam factor is higher and the foam density is lower in the former. This was confirmed by the weight and volume of the test samples: the loose specimens showed a foam density $\rho_{foam}$ of approximately 0.53 g/cm$^3$ ($f_{foam} = 2.37$), whereas for the dense specimens $\rho_{foam} = 0.68$ g/cm$^3$ ($f_{foam} = 1.84$) was determined. A foaming factor of about two ($f_{foam} \approx 2$), which was achieved in the soil $fGr$, implies halving the runtime of the injection pumps and halving the amount of injected material in comparison with cementitious grout. This result is beneficial from the operational and economic point of view, in particular for construction projects with extensive injection measures.

### *Influence of the Curing Time*

To investigate the influence of curing time $t_{cu}$ uniaxial compression tests with $t_{cu} = 2$ h, 7 days, and 28 days after specimen preparation were performed on foam-grouted $fGr$. The test results are shown in Figs. 11(a and b) for $I_D = 0.5$ medium dense and $I_D = 0.85$ dense relative density, respectively.

Despite the small deviations, the stress–strain responses determined after 2 h, 7 days, and 28 days are similar for both initial relative densities. No influence of the curing time on the stress–strain behavior was observed for the foam-grouted $fGr$. High strengths were achieved just after 2 h of curing. This is a significant difference from the behavior of soils grouted with hydraulic binders, which show a considerable increase of strength after 7 days, 28 days, or even longer curing time (Kainrath 2017). The strength of gravel injected with silicate foam after 2 h of curing is similar to the strength of cement-injected soil after 28 days of curing as shown [e.g., by the results of Kainrath (2017)]. To our knowledge, injection material that provides comparable early age strength is rare.

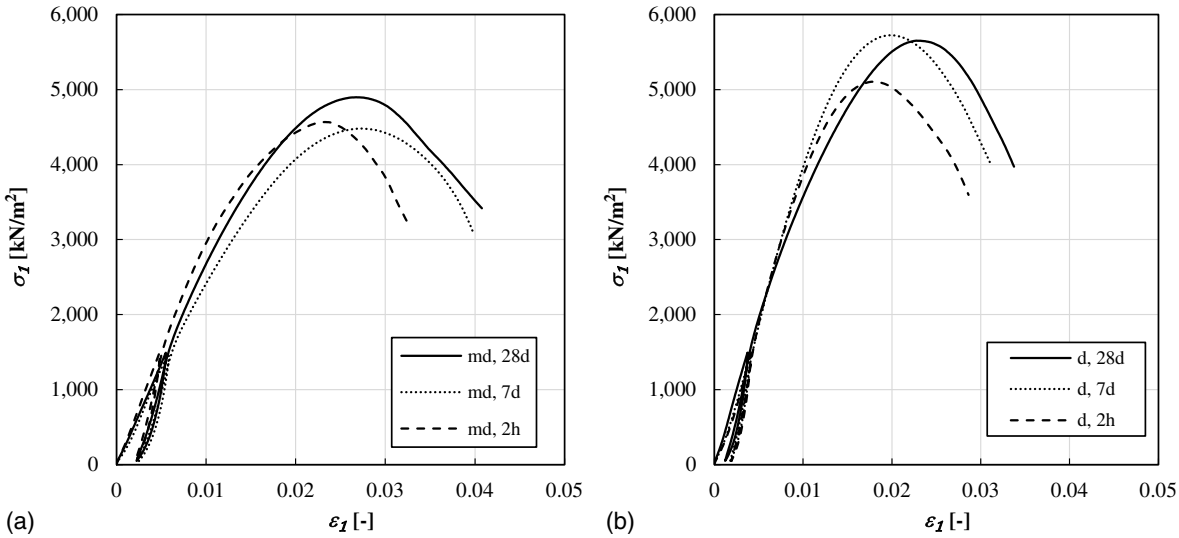


**Fig. 11.** Uniaxial compression tests on foam grouted $fGr$ with varying curing times for: (a) medium dense; and (b) dense relative density at constant rate of strain $\dot{\varepsilon} = 1.0\%/\text{min}$.

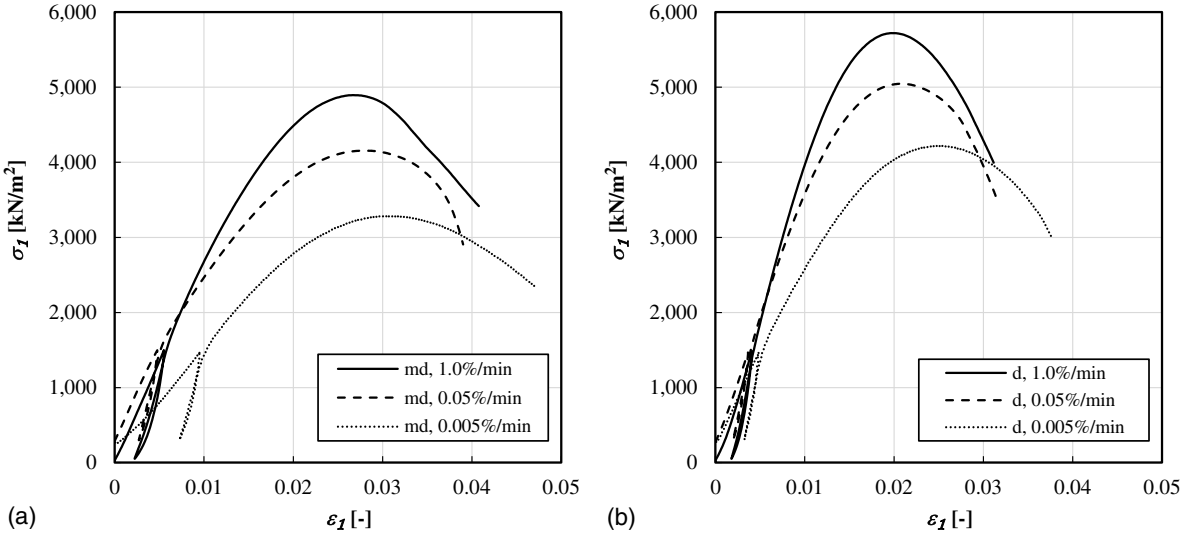


**Fig. 12.** Uniaxial compression tests on foam-grouted $fGr$ with different strain rates: (a) medium dense; and (b) dense relative density.

### *Influence of the Strain Rate*

To investigate the influence of the loading strain rate, uniaxial compression tests with $\dot{\varepsilon} = 1.0\%/\text{min}$, $0.05\%/\text{min}$, and $0.005\%/\text{min}$ were performed on foam-injected $fGr$. Figs. 12(a and b) show the test results for medium dense and dense initial relative density. In the investigated range, the strength and stiffness increase with an increasing strain rate. As the rate dependence of coarse-grained soil is commonly negligible, the observed rate dependence can be assigned predominately to the foam component. The rate dependence of the foam results from a thermally activated process, as described in the section "Foam." Similar material behavior was observed for other composite materials as silicate-stabilized sand (Koenzen 1975; Stetzler-Kaufmann 1983; Gartung 1976; Schubert 1985; Clough et al. 1979), frozen soil (Ting et al. 1983; Andersen et al. 1995; Arenson et al. 2004), and concrete (Bischoff and Perry 1991; Cusatis 2011).

Fig. 13 shows the unconfined compressive strength $q_u$ as a function of the strain rate $\dot{\varepsilon}$. Despite some scatter of the experimental results, the relationship between $q_u$ and $\dot{\varepsilon}$ is linear in a semilogarithmic scale. Therefore, to determine the appropriate compressive strength of the grouted soil to be used in a geotechnical application, a conservative strain rate must be estimated based on the expected load evolution.

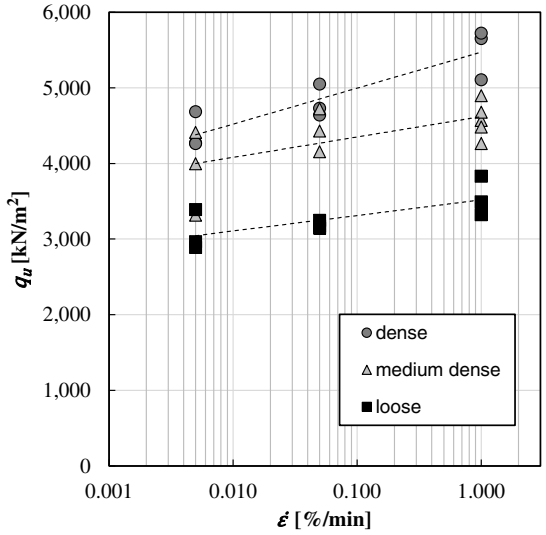


**Fig. 13.** Unconfined compressive strength $q_u$ as a function of the strain rate $\dot{\varepsilon}$ for foam-injected $fGr$.

### *Influence of the Grain Size*

To investigate the influence of grain size, uniaxial compression tests were performed on foam-grouted $fGr$ and $mGr$. During these experiments, the volumetric deformation behavior of the test specimens was examined with the help of circumferential deformation sensors. Fig. 14 presents the results of uniaxial compression tests performed on foam-grouted $fGr$ and $mGr$ at a constant strain rate of $\dot{\varepsilon} = 0.05\%/\text{min}$. Both soils were tested for loose ($I_D = 0.15$) and dense ($I_D = 0.85$) initial relative density. Once the maximum stress was reached, the circumferential LVDTs were removed to prevent damage of the sensors in the event of an abrupt failure of the sample.

The test results indicate that the mechanical response of the investigated composite material also depends on particle size. The strength of foam-grouted $fGr$ is about twice as high as that of the $mGr$ specimens. Two main mechanisms contribute to the observed response:

1. The two gravels investigated exhibit a ratio of the mass-specific surfaces of $fGr$ and $mGr$ of about 2.3. The smaller the grain size and higher the soil density, the larger is the adhesion surface between soil and foam, improving the load transfer in the composite as well as the shear strength. Hutchinson (1963) similarly investigated the mechanical properties of 11 different cement-injected sands with varying granulometric properties. He concluded that the mass-specific surface has a significant influence on the mechanical behavior of cemented sands.
2. The mean pore size in the soil $mGr$ is larger than in the soil $fGr$, enabling larger foam cells to develop in this gravel, in turn resulting in a lower foam density. Accordingly, the strength of the foam-injected $fGr$ samples exceeds the strength of the $mGr$ samples.

For both cohesionless soils, the stiffness in the quasi-linear part of the stress–strain relationship appears to depend only on the initial density. As can be seen in Fig. 14, the samples show the typical volumetric behavior observed in uniaxial and triaxial tests on cemented, frozen, and grouted granular soils. Owing to cracks and

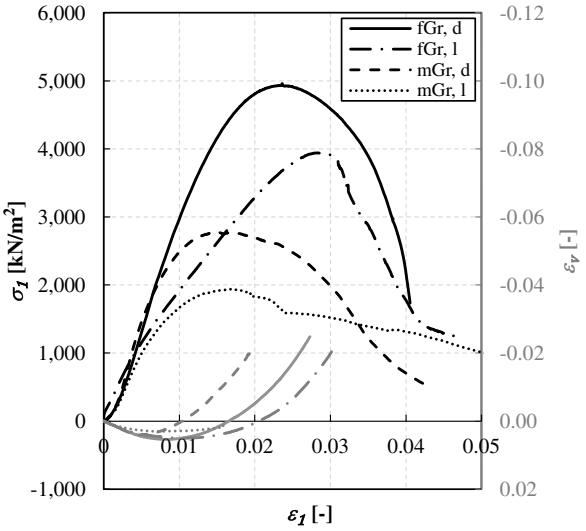


**Fig. 14.** Stress–strain and volumetric behavior of foam-injected $fGr$ and $mGr$ for loose ($I_D = 0.15$) and dense ($I_D = 0.85$) initial relative density.

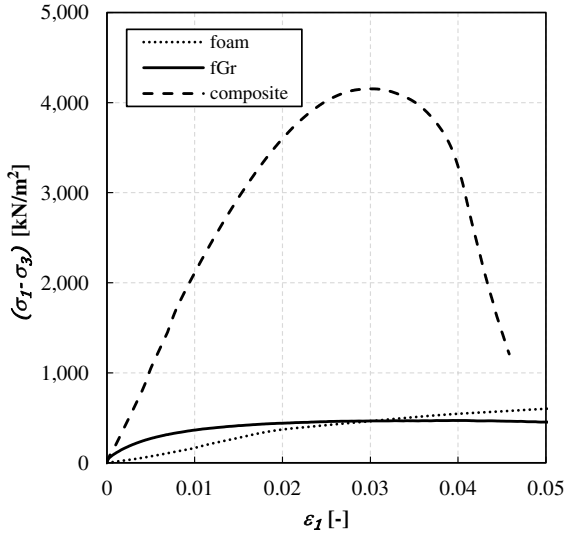


**Fig. 15.** Comparison of stress–strain relationships for the soil–foam composite, the silicate foam, and the natural fine gravel.

shear localization, measurements of radial deformations could not be continued after the peak. The axial strain required to achieve the maximum strength is lower for the medium gravel than for the fine gravel.

## Enhancement of Mechanical Behavior

To evaluate the improvement of mechanical properties caused by the foam injection, we compared the results from the natural fine gravel $fGr$, the foam, and the foam-grouted $fGr$ for similar, but not exactly the same, testing conditions. The following samples and test conditions were used for the comparison:

- Silicate foam: $\rho_{foam} = 0.22\,\mathrm{g/cm^3}$, $\dot{\varepsilon} = 10\%/\mathrm{min}$, $\sigma_3 = 0\,\mathrm{kN/m^2}$
- Fine gravel fGr: $I_D = 0.55$, $\dot{\varepsilon} = 0.05\%/\mathrm{min}$, $\sigma_3 = 100\ \mathrm{kN/m^2}$
- Foam-injected fine gravel: $I_D = 0.5$, $\dot{\varepsilon} = 0.05\%/\mathrm{min}$, $\rho_{foam} = 0.6\ \mathrm{g/cm^3}$, $\sigma_3 = 100\ \mathrm{kN/m^2}$

The stress–strain relationships are presented in Fig. 15. The strength and the stiffness of the grouted soil are significantly higher than those of the individual components, as observed for other composite materials. The peak strength of the natural soil and the composite occur in a comparable strain range between 0.02 and 0.035. After the peak ($\varepsilon \geq 0.032$), the composite shows gradual softening, whereas softening of the soil is less pronounced and strength of the pure foam is still increasing. It must be noted that the foam density in the composite is about 3 times higher than that of the pure foam. Nevertheless, the significant increase of the strength of the composite cannot be justified by an increase of strength of the foam. As mentioned in the "Introduction," two main mechanisms are considered responsible for the enhancement of the mechanical properties of grouted soils. On the one hand, the foam induces a bonding of the grains (cohesion). We assume that the bonding forces primarily depend on the achieved foam density and specific surface of the grains. On the other hand, the foam prevents grain rearrangements (dilatancy) of the granular skeleton leading to the development of larger grain-to-grain forces during shearing. With respect to the original granular soil, we assume that the larger the dilatancy of the ungrouted granular material at the limit state, the more significant the increase of the grouted soil strength will be. Additional experimental investigations are being planned to assess the two postulated enhancing mechanisms.

## Uniaxial Creep Tests

For further investigation of the time-dependent material behavior of foam-grouted soils, monotonous uniaxial creep tests with varying stress levels ($40\%/q_u, 60\%/q_u, 80\%/q_u$) were carried out. The unconfined compressive strength $q_u = 5544\ \mathrm{kN/m^2}$ at a strain rate of $\dot{\varepsilon} = 1.0\%/\mathrm{min}$ was selected as the reference value to define the applied stresses. The respective stress was kept constant for the period of 1 week or until creep failure occurred. The following examples of applications can be addressed with stresses in the applied range (up to 4.4 MPa): ground improvement of the soil pillar between twin tunnels, umbrella arch methods, stabilization of the tunnel face, underpinnings, and anchor grouting.

The test results are shown for foam-injected $fGr$ and $mGr$ in Figs. 16(a–d). Both of the sample types ($fGr$ and $mGr$) were tested for dense ($I_D = 0.85$) or loose ($I_D = 0.15$) relative density. The strain versus time graphs in Figs. 16(a and b) use a linear scale, whereas the strain-rate versus time graphs in Figs. 16(c and d) are plotted in double logarithmic scale.

The creep behavior of both composite sample types ($fGr$ and $mGr$) is characterized by primary, secondary and tertiary creep phases, as it is for the pure foam [Figs. 1(a and b)]. Creep deformations increase with increasing axial stress as shown in Figs. 16(a and b). At the lower stress levels (40 and 60% of $q_u$), the creep strain rate $\dot{\varepsilon}$ decreases consistently over time. The decrease of the strain rate is approximately linear in a double logarithmic scale over the entire duration of the test (7 days). A decreasing strain rate during creep indicates stable material behavior.

In contrast, an increase of the creep strain rate over time inevitably leads to the collapse of the sample, as observed at the stress level of 80% of $q_u$ for both soils regardless of the initial soil density. At this stress level ($80\% \cdot q_u$), the strain rate initially decreases with time until a minimum value of $\dot{\varepsilon}_{min}$ is achieved. Afterward, the strain rate increases until the samples collapse, as shown in Figs. 16(c and d). The time required to reach the turning point of the strain-rate is $t_f$ and the corresponding strain $\varepsilon_{f,c}$. Relevant results of the creep tests are summarized in Table 3.

The time $t_f$ depends on the initial relative density of the soil: the dense specimens ($I_D = 0.85$) reached the turning point earlier than the loose ($I_D = 0.15$) ones. A single localized shear plane was observed in the dense specimens, while many small, randomly

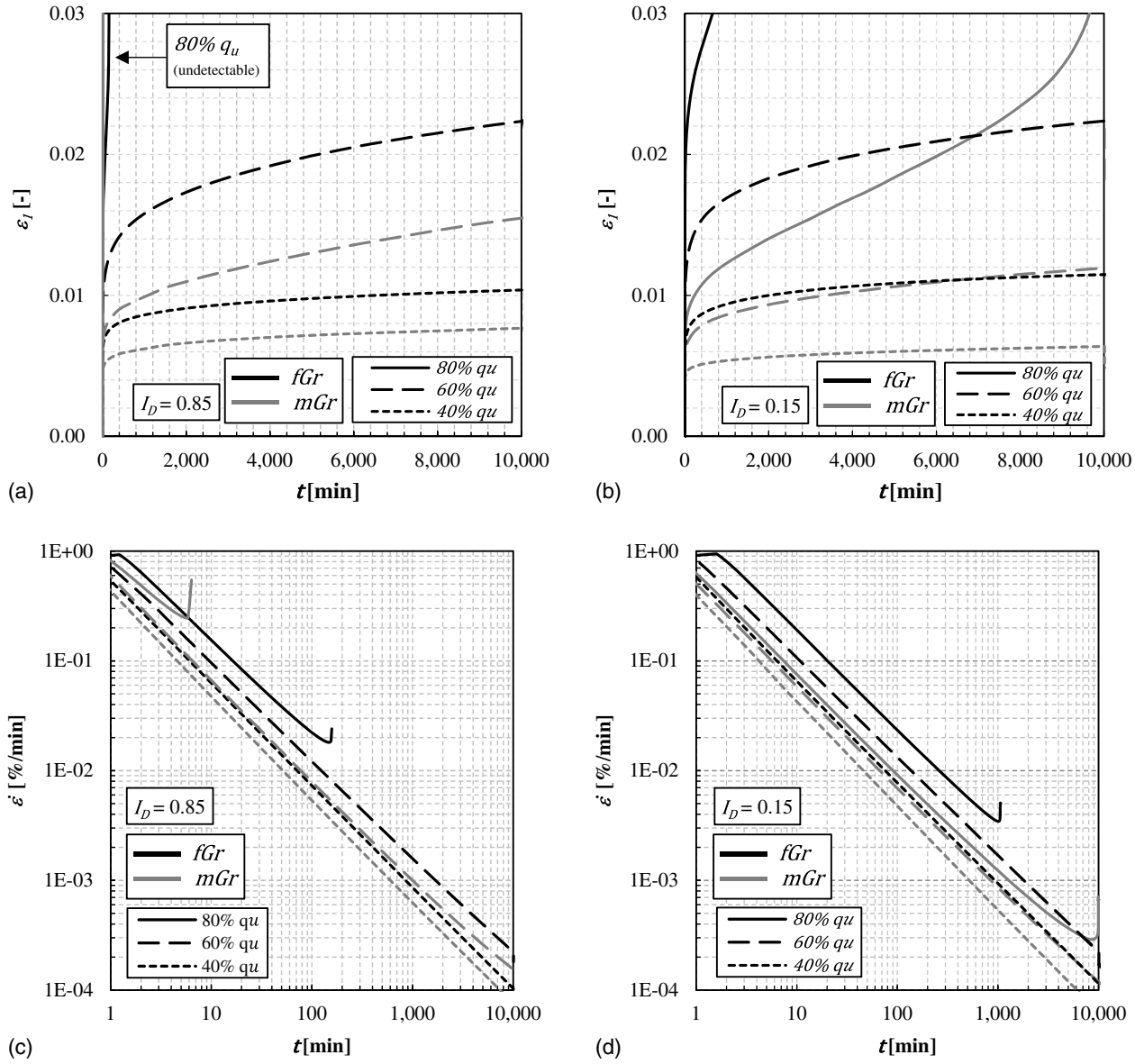


**Fig. 16.** Uniaxial creep tests for foam-injected $fGr$ and $mGr$ with varying load levels: (a and c) for $I_D = 0.85$; and (b and d) for $I_D = 0.15$.

**Table 3.** Results of the uniaxial single-step creep tests on foam-injected soil

| Soil | $I_D$ | $\sigma/q_u$ (%) | $\sigma$ (kN/m$^2$) | $\dot{\varepsilon}_{min}$ (%/min) | $t_f$ (min) | $\varepsilon_{f,c}$ |
|---|---|---|---|---|---|---|
| $fGr$ | 0.85 | 40 | 2,220 | — | — | — |
| | | 60 | 3,325 | — | — | — |
| | | 80 | 4,435 | $1.8 \times 10^{-2}$ | 145 | 0.0263 |
| | 0.15 | 40 | 1,350 | — | — | — |
| | | 60 | 2,030 | — | — | — |
| | | 80 | 2,700 | $3.5 \times 10^{-3}$ | 1,007 | 0.0347 |
| $mGr$ | 0.85 | 40 | 1,250 | — | — | — |
| | | 60 | 1,880 | — | — | — |
| | | 80 | 2,505 | $2.5 \times 10^{-1}$ | 6 | 0.0138 |
| | 0.15 | 40 | 695 | — | — | — |
| | | 60 | 1,040 | — | — | — |
| | | 80 | 1,390 | $2.9 \times 10^{-4}$ | 8,619 | 0.0249 |

Note: $\dot{\varepsilon}_{min}$ = minimum strain rate; $t_f$ = time to failure that is determined at the minimum of creep rate, when creep failure occurred; and $\varepsilon_{f,c}$ = strain at $t_f$.

distributed cracks occurred in the loose specimens. The creep strain at the turning point $\varepsilon_f$ is about 0.03 for the foam-grouted $fGr$ and 0.02 for the foam-grouted $mGr$. These values are comparable with the values required to mobilize the material strength in the strain-rate controlled uniaxial compression tests and suggest that creep failure might be connected to a threshold shear strain. As long as the threshold strain is not reached, the strain-rate decreases and the mechanical behavior is stable, as is the case in the creep tests with vertical stress corresponding to 40% and 60% of $q_u$. Currently, we assume that creep failure can occur even at a stress level of 60% of $q_u$ and possibly 40% of $q_u$ if the creep time is sufficient to achieve the corresponding threshold strain. Nonetheless, further experimental evidence is required to clarify this topic.

## Description of Uniaxial Strength and Stiffness Using the Porosity–Binder Concept

The uniaxial compression test results have shown that the mechanical behavior ($q_u$, $E$) of foam-grouted soils depends on soil and foam

density. In this section, we apply the porosity–binder concept ($n/B$-index) to describe this dependency. Hutchinson (1963) was one of the first authors who correlated strength and the porosity–cement ratio of cement-stabilized sands in terms of a power function. Until now, the $n/B$-index has been used to correlate the tensile, uniaxial, and triaxial strength and stiffness of different binder-treated soils (Consoli et al. 2007, 2010, 2011, 2017b, 2018). The porosity–binder concept has not yet been applied to grouted soil, particularly foam-grouted soil. A detailed description of the porosity–binder concept and the theoretical background is given by Henzinger and Schömig (2020). Probably the most relevant form of the porosity–binder concept is shown in Eq. (10), which was first proposed by Consoli et al. (2007)

$$q_u = A_{pb}\left(\frac{n}{B_{iv}^x}\right)^{-\alpha} \tag{10}$$

where, as illustrated in Fig. 17, $n$ is the porosity of the grouted material (the ratio of the volume of voids to the total volume); $B_{iv}$ is the volumetric percentage of the bonding agent (the ratio of volume of the bonding agent and the total volume); and $A_{pb}$, $\alpha$, and $x$ are model parameters to be determined experimentally.

By measuring volume $V_{sp}$ and weight $m_{sp}$ of the tested specimens and knowing the initial dry density of soil $\rho_d$, $n$ and $B_{iv}$ can be determined according to

$$m_{foam} = m_{sp} - \rho_d/V_{sp} \tag{11}$$

$$n = \frac{V_{sp} - m_{foam}/\rho_{fluid} - m_d/\rho_S}{V_{sp}} \tag{12}$$

$$B_{iv} = \frac{m_{foam}/\rho_{fluid}}{V_{sp}} \tag{13}$$

where $m_{foam}$ is the mass of the foam in the specimen; and $m_d$ is the dry mass of soil. To determine the coefficients $A_{pb}$, $\alpha$, and $x$, the experimental values of $q_u$ are plotted against the calculated values $n/B_{iv}$. The three coefficients are determined iteratively for the coefficient of determination $R^2$ of Eq. (10) to achieve a maximum (Henzinger and Schömig 2020). This procedure has been applied to the test series of foam-grouted $fGr$ with different initial density and varying strain rate. The parameters were determined for uniaxial compressive strength $q_u$ and stiffness $E$. Table 4 includes values of the coefficients of Eq. (10) for $q_u$ and $E$ for different strain rates. The stiffness $E$ was evaluated in the linear range of the stress–strain diagram between 20% and 60% of $q_u$.

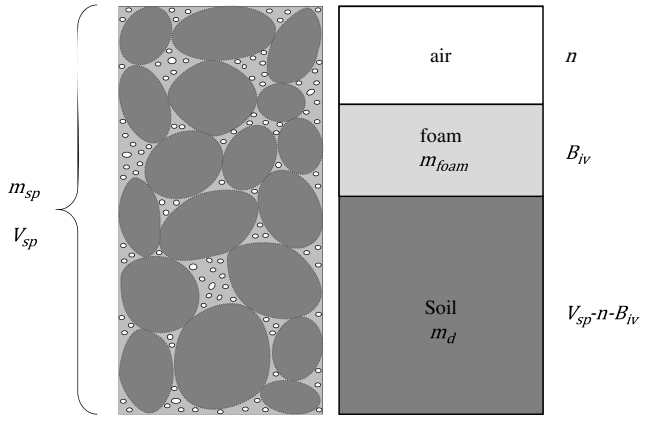


**Fig. 17.** Schematic illustration of the porosity–binder concept for foam-injected soil specimens.

**Table 4.** Parameterization of Eq. (10) for uniaxial compressive strength $q_u$ and stiffness $E$ of foam-grouted $fGr$

| fGr | $\dot{\varepsilon}$ (mm/min) | U | $A_{pb}$ (kN/m$^2$) | x | $\alpha$ | $R^2$ |
|---|---|---|---|---|---|---|
| $q_u$ | 1.000 | 10 | 466.5 | −0.423 | 0.951 | 0.85 |
| | 0.050 | 9 | 387.2 | −0.382 | 1.017 | 0.81 |
| | 0.005 | 9 | 355.2 | −0.365 | 1.031 | 0.86 |
| $E$ | 1.000 | 10 | 1.682 | −0.450 | 2.105 | 0.92 |
| | 0.050 | 9 | 1.599 | −0.468 | 2.071 | 0.83 |
| | 0.005 | 9 | 1.208 | −0.441 | 2.148 | 0.83 |

Note: $U$ = number of tested samples.

Although the number of data for each strain rate is currently limited, the values for the coefficient of determination ($R^2 \geq 0.81$) demonstrate that the relationship between strength/stiffness, porosity of the grouted soil, and binder percentage (foam density) can be described accurately using Eq. (10). With decreasing strain rate $\dot{\varepsilon}$, mainly the parameter $A_{pb}$ changes, while the exponents $x$ and $\alpha$ remain almost constant in Eq. (10). For $q_u$:$x = [-0.365; -0.432]$ and $\alpha = [0.951; 1.031]$. For $E$:$x = [-0.441; -0.468]$ and $\alpha = [2.071; 2.148]$. Therefore, both exponents $x$ and $\alpha$ can be assumed to be approximately independent of the strain rate. Figs. 18(a and b) illustrate the evaluation of $q_u$ and $E$ as a function of the porosity–binder concept for unified $x$- and $\alpha$- values. The adopted $x$- and $\alpha$- values are in the range of the values presented in Table 4 and lead to the highest possible coefficient of determination $R^2$.

Using the unified exponents $x$ and $\alpha$, a single relationship between normalized values $\overline{q_u}$ and $\bar{E}$ and the porosity–binder index can be determined (Consoli et al. 2016, 2017a), as shown in Eq. (14) for $\overline{q_u}$

$$\overline{q_u} = \frac{q_u}{q_{u(\Delta)}} = \frac{A_{pb}\left[\frac{n}{B_{iv}^x}\right]^{-\alpha}}{A_{pb}[\nabla]^{-\alpha}} = \frac{\left[\frac{n}{B_{iv}^x}\right]^{-\alpha}}{[\nabla]^{-\alpha}} \tag{14}$$

The normalization is performed for an arbitrarily chosen value of $(n/B_{iv}^x) = \nabla = 0.10$. Figs. 19(a and b) show the normalized values for the strain rates $\dot{\varepsilon} = 1.0\%/\text{min}$, $\dot{\varepsilon} = 0.05\%/\text{min}$, and $\dot{\varepsilon} = 0.005\%/\text{min}$.

Despite the limited data base with a total number of 28 test results, relatively high correlation coefficients $R^2$ for $q_u$ and $E$ are achieved. Based on the normalized Eq. (13), a minimum of three tests with a single strain rate and one test for each additionally considered strain-rate are required to estimate the coefficients $x$, $\alpha$, and $A_{pb}$. Then, Eq. (13) can be used to predict the compressive strength and stiffness in situ as a function of the in situ density of the soil and the density of the injected foam. For the soil $fGr$, the following relationships were derived from the experimental data:

$$q_u = A_{pb}\left(\frac{n}{B_{iv}^{-0.39}}\right)^{-1.00} A_{pb} = \left\{\begin{array}{c} 437.7 \rightarrow \dot{\varepsilon} = 1.0\%/min \\ 398.5 \rightarrow \dot{\varepsilon} = 0.05\%/min \\ 365.7 \rightarrow \dot{\varepsilon} = 0.005\%/min \end{array}\right\} \tag{15}$$

$$E = A_{pb}\left(\frac{n}{B_{iv}^{-0.45}}\right)^{-2.11} A_{pb} = \left\{\begin{array}{c} 1.649 \rightarrow \dot{\varepsilon} = 1.0\%/min \\ 1.427 \rightarrow \dot{\varepsilon} = 0.05\%/min \\ 1.285 \rightarrow \dot{\varepsilon} = 0.005\%/min \end{array}\right\} \tag{16}$$

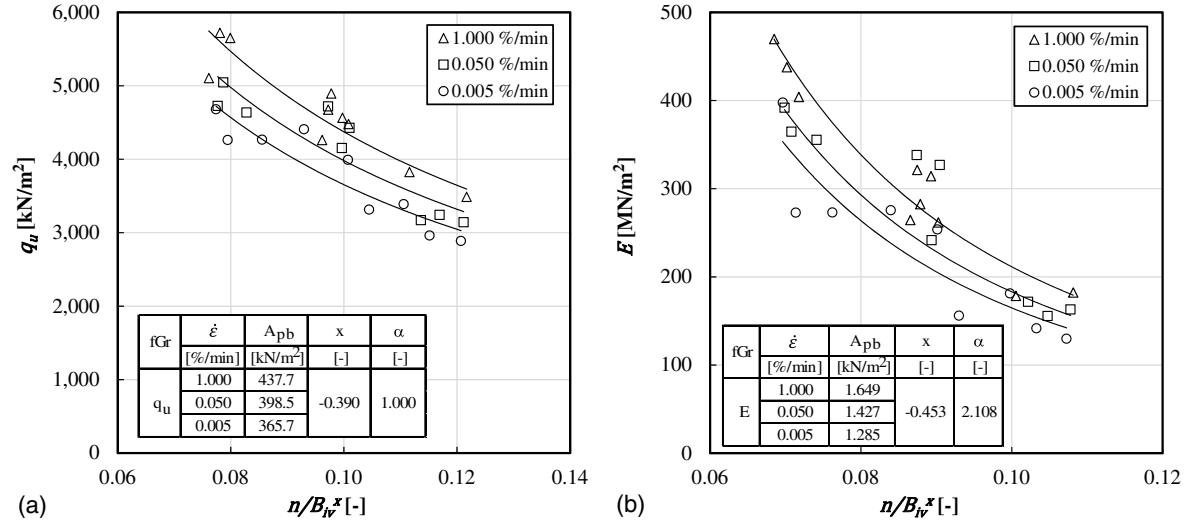


**Fig. 18.** Porosity–binder concept of foam-injected $fGr$ for unified $x$- and $\alpha$- values: (a) unconfined compressive strength $q_u$; and (b) stiffness $E$.

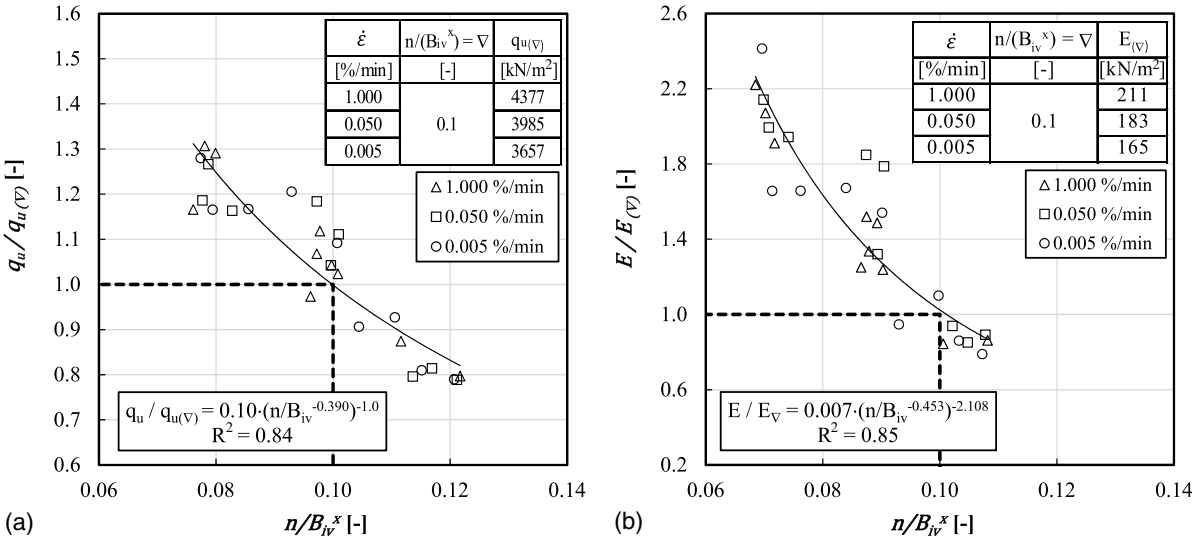


**Fig. 19.** Normalization of: (a) $q_u$; and (b) $E$ according to Eq. (14) for foam-injected $fGr$.

## Conclusions

In this paper, the mechanical behavior of two foam-grouted gravels was investigated by means of uniaxial compression and uniaxial creep tests. In order to achieve reproducibility, a technique to prepare composite specimens with controlled initial soil density was developed and successfully validated. The results show the mechanical behavior is enhanced by the foam grouting. The strength and the stiffness of the grouted soil is significantly higher than those of the individual components. The enhancement of the mechanical properties is mainly caused by the bonding of the grains (cohesion) and the prevention of grain rearrangements (dilatancy) of the granular skeleton induced by the foam. The volumetric deformations reveal dilatant behavior for both the loose and the dense samples. In contrast to soil improved with hydraulic binders, the strength of foam-grouted soils developed much faster. In our experiments, the uniaxial compressive strength was developed after 2 h of curing. Therefore, foam grouting can be especially advantageous in applications in which extremely early age strengths are required (e.g., for the stabilization of tunnel faces during excavation).

In general, soil–foam composites show an elasto-viscoplastic mechanical behavior. The experimental results indicate that the uniaxial compressive strength increases with increasing initial density of the soil, foam density, and shearing rate. The rate-dependence of the soil–foam composites results predominantly from the viscous behavior of the foam, which can be described as a thermally activated process at the micro-level. During creep, the strain rate decreases linearly with time in a double logarithmic scale. A transition from secondary to tertiary creep occurs after a certain time, depending on the acting stress. At the turning point, the strain rate achieves a minimum and starts to rapidly grow with time until the sample collapses. Within the creep time of 7 days, the turning point was only achieved for a stress level of 80% $q_u$. In addition, it is observed that the strain at the turning point $\varepsilon_{f,c}$ is similar to the strain $\varepsilon_{f,s}$ required to mobilize the material strength under shearing in the strain-rate controlled uniaxial compression tests. Based on

this observation, we currently assume that the failure during creep will occur only when $\varepsilon_{f,c}$ is achieved. As a first approximation, $\varepsilon_{f,c} \approx \varepsilon_{f,s}$ can be taken. In the creep tests of 40% and 60% $q_u$, the creep strain $\varepsilon_1 \ll \varepsilon_{f,s}$ at the end of the 7 days creep time and, consequently, no creep failure was observed. Further investigation is required to support our preliminary assumptions regarding the creep behavior of foam-grouted soils.

Finally, it was shown that the porosity–binder concept can be used to predict the strength as well as the stiffness of foam-grouted cohesionless soils as function of soil density, foam density, and strain rate. The porosity–binder relationship can be calibrated with a small number of laboratory tests and used to estimate the in situ strength and stiffness of foam-injected soils.

## Data Availability Statement

Some or all data, models, or code that support the findings of this study are available from the corresponding author upon reasonable request.

## Acknowledgments

The authors wish to express their gratitude to Federal Ministry for Economic Affairs and Energy and TPH Bausysteme GmbH for their financial support of this research.

## Notation

*The following symbols are used in this paper:*

$A, A'$ = area;
$A_0$ = initial cross-sectional area;
$B_{iv}$ = volumetric percentage of the bonding agent;
$C_C$ = curvature number;
$C_U$ = uniformity coefficient;
$D$ = diameter of the specimen;
$d_{10}$, $d_{30}$, $d_{50}$, $d_{60}$ = particle diameter at 10%, 30%, 50%, and 60% in the cumulative distribution;
$E$ = Young's modulus;
$e$ = void ratio;
$e_{max}$ = maximum void ratio;
$e_{min}$ = minimum void ratio;
$f_{foam}$ = foam factor;
$fGr$ = fine gravel;
$H$ = height of the specimen;
$I_D$ = relative density of the soil;
$K$ = pre-exponential factor;
$k$ = hydraulic permeability;
$m_d$ = dry mass of the soil;
$m_{foam}$ = mass of the foam;
$mGr$ = medium gravel;
$m_{sp}$ = weight of the specimen;
$N$ = creep exponent;
$n$ = percentage of voids within the composite;
$Q$ = the creep activation energy;
$q_u$ = uniaxial compression strength;
$R$ = gas constant;
$R^2$ = coefficient of determination;
$r_0$ = initial radius of the specimen;
$S_m$ = mass specific surface;
$T$ = temperature;
$t$ = time;
$t_{cu}$ = curing time;
$t_f$ = time to failure;
$U$ = number of tested samples;
$u$ = perimeter of the specimen;
$V_{foam}$ = volume of the foam including the gas-filled cells;
$V_{sp}$ = volume of the specimen;
$x$, $\alpha$, $A_{pb}$ = parameters of the porosity binder concept;
$x_{area}$ = equivalent diameter;
$\nabla$ = arbitrarily chosen $n/B_{iv}$-value;
$\dot{\varepsilon}$ = strain rate;
$\varepsilon_{f,c}$ = creep strain at the turning point;
$\varepsilon_{f,s}$ = strain at the maximum shear stress;
$\dot{\varepsilon}_{min}$ = minimum strain rate;
$\varepsilon_v$ = volumetric strain;
$\varepsilon_1$ = axial strain;
$\varepsilon_3$ = radial strain;
$\eta$ = dynamic viscosity;
$\rho$ = density;
$\rho_{fluid}$ = density of the fluid foam;
$\rho_{foam}$ = foam density;
$\rho_S$ = density of solid particles;
$\sigma$ = stress;
$\sigma/q_u$ = stress level for the uniaxial creep tests;
$\sigma_0$, $\dot{\varepsilon}_0$ = constants characterizing the creep of the solid making the foam;
$\sigma_1$ = vertical stress; and
$\sigma_3$ = confining pressure.

## References

Andersen, G. R., C. W. Swan, C. C. Ladd, and J. T. Germaine. 1995. "Small-strain behavior of frozen sand in triaxial compression." *Can. Geotech. J.* 32 (3): 428–451. https://doi.org/10.1139/t95-047.

Andrews, E. W., L. J. Gibson, and M. F. Ashby. 1999a. "The creep of cellular solids." *Acta Mater.* 47 (10): 2853–2863. https://doi.org/10.1016/S1359-6454(99)00150-0.

Andrews, E. W., J.-S. Huang, and L. J. Gibson. 1999b. "Creep behavior of a closed-cell aluminum foam." *Acta Mater.* 47 (10): 2927–2935. https://doi.org/10.1016/S1359-6454(99)00161-5.

Arenson, L. U., M. M. Johansen, and S. M. Springman. 2004. "Effects of volumetric ice content and strain rate on shear strength under triaxial conditions for frozen soil samples." *Permafrost Periglacial Processes* 15 (3): 261–271. https://doi.org/10.1002/ppp.498.

Ashby, M. F. 1983. "The mechanical properties of cellular solids." *Metall. Trans. A* 14 (9): 1755–1769. https://doi.org/10.1007/BF02645546.

Ashby, M. F. 2006. "The properties of foams and lattices." *Philos. Trans. R. Soc. London, Ser. A: Math. Phys. Eng. Sci.* 364 (1838): 15–30. https://doi.org/10.1098/rsta.2005.1678.

Bischoff, P. H., and S. H. Perry. 1991. "Compressive behaviour of concrete at high strain rates." *Mater. Struct.* 24 (6): 425–450. https://doi.org/10.1007/BF02472016.

Bodi, J., Z. Bodi, J. Scucka, and P. Martinec. 2012. "Polyurethane grouting technologies." In *Polyurethane*, edited by F. Zafar, 307–336. London: InTech.

Bruce, D. A., C. S. El Mohtar, M. J. Byle, P. Gazzarrini, L. F. Johnsen, and D. R. Thomas. 2017. *Grouting 2017: Case histories. Geotechnical special publications v.287*. Reston, VA: ASCE.

Budach, C., and M. Thewes. 2015. "Application ranges of EPB shields in coarse ground based on laboratory research." *Tunnelling Underground Space Technol.* 50 (2011): 296–304. https://doi.org/10.1016/j.tust.2015.08.006.

Burteau, A., J.-D. Bartout, Y. Bienvenu, and S. Forest. 2014. "On the creep deformation of nickel foams under compression." *C.R. Phys.* 15 (8–9): 705–718. https://doi.org/10.1016/j.crhy.2014.09.004.

Cambefort, H. 1969. *Bodeninjektionstechnik: Einpressungen in Untergrund Und Bauwerke*. Wiesbaden und Berlin: Bauverlag GmbH.

Christopher, B., D. Atmatzidis, and R. Krizek. 1989. "Laboratory testing of chemically grouted sand." *Geotech. Test. J.* 12 (2): 109. https://doi.org/10.1520/GTJ10685J.

Clough, G. W., W. M. Kück, and G. Kasali. 1979. "Silicate-stabilized sands." *J. Geotech. Eng. Div.* 105 (1): 65–82. https://doi.org/10.1061/AJGEB6.0000760.

Consoli, N. C., R. C. Cruz, M. F. Floss, and L. Festugato. 2010. "Parameters controlling tensile and compressive strength of artificially cemented sand." *J. Geotech. Geoenviron. Eng.* 136 (5): 759–763. https://doi.org/10.1061/(ASCE)GT.1943-5606.0000278.

Consoli, N. C., A. P. da Silva, H. P. Nierwinski, and J. Sosnoski. 2018. "Durability, strength, and stiffness of compacted gold tailings–cement mixes." *Can. Geotech. J.* 55 (4): 486–494. https://doi.org/10.1139/cgj-2016-0391.

Consoli, N. C., D. Foppa, L. Festugato, and K. S. Heineck. 2007. "Key parameters for strength control of artificially cemented soils." *J. Geotech. Geoenviron. Eng.* 133 (2): 197–205. https://doi.org/10.1061/(ASCE)1090-0241(2007)133:2(197).

Consoli, N. C., L. D. S. Lopes Jr, P. D. M. Prietto, L. Festugato, and R. C. Cruz. 2011. "Variables controlling stiffness and strength of lime-stabilized soils." *J. Geotech. Geoenviron. Eng.* 137 (6): 628–632. https://doi.org/10.1061/(ASCE)GT.1943-5606.0000470.

Consoli, N. C., S. F. V. Marques, M. F. Floss, and L. Festugato. 2017a. "Broad-spectrum empirical correlation determining tensile and compressive strength of cement-bonded clean granular soils." *J. Mater. Civ. Eng.* 29 (6): 06017004. https://doi.org/10.1061/(ASCE)MT.1943-5533.0001858.

Consoli, N. C., R. A. Quiñónez, L. E. González, and R. A. López. 2017b. "Influence of molding moisture content and porosity/cement index on stiffness, strength, and failure envelopes of artificially cemented fine-grained soils." *J. Mater. Civ. Eng.* 29 (5): 04016277. https://doi.org/10.1061/(ASCE)MT.1943-5533.0001819.

Consoli, N. C., R. A. Q. Samaniego, S. F. V. Marques, G. I. Venson, E. Pasche, and L. E. G. Velásquez. 2016. "Single model establishing strength of dispersive clay treated with distinct binders." *Can. Geotech. J.* 53 (12): 2072–2079. https://doi.org/10.1139/cgj-2015-0606.

Couteau, O., and D. C. Dunand. 2008. "Creep of aluminum syntactic foams." *Mater. Sci. Eng., A* 488 (1–2): 573–579. https://doi.org/10.1016/j.msea.2008.01.022.

Cusatis, G. 2011. "Strain-rate effects on concrete behavior." *Int. J. Impact Eng.* 38 (4): 162–170. https://doi.org/10.1016/j.ijimpeng.2010.10.030.

DIN (Deutsches Institut für Normung e.V.). 2018. *Geotechnische Erkundung und Untersuchung—Laborversuche an Bodenproben—Teil 7: Einaxialer Druckversuch*. DIN EN ISO 17892-7. Berlin: Beuth Verlag GmbH.

Diologent, F., Y. Conde, R. Goodall, and A. Mortensen. 2009. "Microstructure, strength and creep of aluminium-nickel open cell foam." *Philos. Mag.* 89 (13): 1121–1139. https://doi.org/10.1080/14786430902915396.

Eyring, H. 1936. "Viscosity, plasticity, and diffusion as examples of absolute reaction rates." *J. Chem. Phys.* 4 (4): 283–291. https://doi.org/10.1063/1.1749836.

Fillibeck, J., N. Vogt, and M. Zaunseder. 2006. "Bau Der U-Bahn-Linie U3 Nord, Los 1 in München - Oberflächensetzungen Beim Spritzbetonvortrieb Mit Schirmgewölbesicherungen." *Bauingenieur* 81: 359–366.

Garshol, K. F. 2002. "Vorinjektion im Tunnelbau—Eine vernünftige Maßnahme." In *Beiträge Zum 17. Christian Vedder Kolloquium: Injektionen in Boden Und Fels*, edited by G. Riedmüller, W. Schubert, and S. Semperich. Graz, Austria: Technische Universität Graz, Gruppe Geotechnik Graz, Institut für Bodenmechanik und Grundbau.

Gartung, E. 1976. *Grundsatzversuche Mit Silikatgelinjektion im Nürnberger sand*. Nürnberg, Germany: Eigenverlag LGA. Veröffentlichungen des Grundbauinstituts der Landesgewerbeanstalt Bayern.

Gibson, L. J., and M. F. Ashby. 2014. *Cellular solids*. Cambridge, UK: Cambridge University Press.

Henzinger, C., and P. Schömig. 2020. "Prognose der Festigkeitsentwicklung Zementbehandelter Böden Mit Dem Porosity/Binder-Index." *geotechnik* 43 (1): 14–25. https://doi.org/10.1002/gete.201900017.

Holter, K.-G., and H.-O. Hognestad. 2012. "Modern pre-injection in underground construction with rapid-setting microcements and colloidal silica—Applications in conventional and TBM-tunnelling." *Geomechanik Tunnelbau* 5 (1): 49–56. https://doi.org/10.1002/geot.201200001.

Hornich, W., and G. Stadler. 2011. *InjektionenGrundbau-Taschenbuch: Teil 2: Geotechnische Verfahren*, edited by K. J. Witt, 159. Berlin: Ernst.

Huang, J. S., and L. J. Gibson. 1991. "Creep of polymer foams." *J. Mater. Sci.* 26 (3): 637–647. https://doi.org/10.1007/BF00588298.

Hutchinson, B. G. 1963. "Granulometric properties of cement stabilized sands." *J. Soil Mech. Found. Div.* 89 (3): 95–102. https://doi.org/10.1061/JSFEAQ.0000522.

Kainrath, A. 2017. "Injektionen Im Lockergestein." Ph.D. dissertation, Institut für Geotechnik, Technische Universität Wien.

Karol, R. H. 2003. *Chemical grouting and soil stabilization*. Hoboken, NJ: Marcel Dekker Inc.

Koenzen, P. J. 1975. "Rheologische Eigenschaften Silikat-Injizierter Sande." Ph.D. dissertation, Institut für Bodenmechanik und Felsmechanik, Karlsruher Institut für Technologie.

Kutzner, C. 1991. *Injektionen im Baugrund*. Stuttgart, Germany: Enke.

Lade, P. 2016. *Triaxial testing of soils*. Hoboken, NJ: Wiley.

Liu, X. X., S. L. Shen, A. Zhou, and Y. S. Xu. 2019. "Evaluation of foam conditioning effect on groundwater inflow at tunnel cutting face." *Int. J. Numer. Anal. Methods Geomech.* 43 (2): 463–481. https://doi.org/10.1002/nag.2871.

Maji, A. K., L. Schreyer, S. Donald, Q. Zuo, and D. Satpathi. 1995. "Mechanical properties of polyurethane-foam impact limiters." *J. Eng. Mech.* 121 (4): 528–540. https://doi.org/10.1061/(ASCE)0733-9399(1995)121:4(528).

Mane, J. V., S. Chandra, S. Sharma, H. Ali, V. M. Chavan, B. S. Manjunath, and R. J. Patel. 2017. "Mechanical property evaluation of polyurethane foam under quasi-static and dynamic strain rates—An experimental study." *Procedia Eng.* 173: 726–731. https://doi.org/10.1016/j.proeng.2016.12.160.

Microtrac Retsch GmbH. 2021. "Particle characterization: Correlation between sieve analysis and image analysis made easy." Accessed January 8, 2021. https://www.microtrac.de/dltmp/www/5e396c09-86c8-42f5-a041-7f30c3c9c754-ad644028a252/wp_DIA_sieving_0718_en.pdf.

Mori, L., M. Mooney, and M. Cha. 2018. "Characterizing the influence of stress on foam conditioned sand for EPB tunneling." *Tunnelling Underground Space Technol.* 71 (1): 454–465. https://doi.org/10.1016/j.tust.2017.09.018.

Nicholson, P. G. 2014. *Soil improvement and ground modification methods: Elsevier Reference Monographs*. Oxford, UK: Elsevier.

Obi, B. E. 2018. "Structure–property relationships of polymeric foams." In *Polymeric foams structure-property-performance*, 189–205. Oxford, UK: Elsevier.

Quebaud, S., M. Sibai, and J. P. Henry. 1998. "Use of chemical foam for improvements in drilling by earth pressure balanced shields in granular soil." *Tunnelling Underground Space Technol.* 13 (2): 173–180. https://doi.org/10.1016/S0886-7798(98)00045-5.

Richeton, J., S. Ahzi, K. S. Vecchio, F. C. Jiang, and R. R. Adharapurapu. 2006. "Influence of temperature and strain rate on the mechanical behavior of three amorphous polymers: Cha-racterization and modeling of the compressive yield stress." *Int. J. Solids Struct.* 43 (7–8): 2318–2335. https://doi.org/10.1016/j.ijsolstr.2005.06.040.

Schubert, A. 1985. "Ein Beitrag Zum Spannungs-Verformungsverhalten Silikatgel-Injizierter Sande." Ph.D. dissertation, Lehrstuhl und Prüfamt für Grundbau, Bodenmechanik und Felsmechanik der Technischen Universität München, Technische Universität München.

Scucka, J., P. Martinec, and K. Soucek. 2015. "Polyurethane grouted gravel type geomaterials—A model study on relations between material structure and physical–mechanical properties." *Geotech. Test. J.* 38 (2): 20140100. https://doi.org/10.1520/GTJ20140100.

Stetzler-Kaufmann, B. 1983. "Stoffverhalten Chemisch Injizierter Sande." Ph.D. dissertation, Institut für Bodenmechanik und Felsmechanik, Karlsruher Institut für Technologie.

Stieß, M. 2009. *Mechanische Verfahrenstechnik—Partikeltechnologie 1*. Berlin, Heidelberg: Springer.

Thewes, M., and C. Budach. 2010. "Soil conditioning with foam during EPB tunnelling. Konditionierung Von Lockergesteinen Bei Erddruckschilden." *Geomechanik Tunnelbau* 3 (3): 256–267. https://doi.org/10.1002/geot.201000023.

Ting, J. M., R. Torrence Martin, and C. C. Ladd. 1983. "Mechanisms of strength for frozen sand." *J. Geotech. Eng.* 109 (10): 1286–1302. https://doi.org/10.1061/(ASCE)0733-9410(1983)109:10(1286).

Tu, Z. H., V. P. W. Shim, and C. T. Lim. 2001. "Plastic deformation modes in rigid polyurethane foam under static loading." *Int. J. Solids Struct.* 38 (50–51): 9267–9279. https://doi.org/10.1016/S0020-7683(01)00213-X.

Valentino, R., E. Romeo, and D. Stevanoni. 2014. "An experimental study on the mechanical behaviour of two polyurethane resins used for geotechnical applications." *Mech. Mater.* 71 (Apr): 101–113. https://doi.org/10.1016/j.mechmat.2014.01.007.

Warner, J. 2004. *Practical handbook of grouting: Soil, rock, and structures*. Hoboken, NJ: Wiley.

Wei, Y., F. Wang, X. Gao, and Y. Zhong. 2017. "Microstructure and fatigue performance of polyurethane grout materials under compression." *J. Mater. Civ. Eng.* 29 (9): 04017101. https://doi.org/10.1061/(ASCE)MT.1943-5533.0001954.

Wu, Y., M. A. Mooney, and M. Cha. 2018. "An experimental examination of foam stability under pressure for EPB TBM tunneling." *Tunnelling Underground Space Technol.* 77 (8–9): 80–93. https://doi.org/10.1016/j.tust.2018.02.011.